Journal of Sound and Vibration (2002) **250**(3), 401–414
doi:10.1006/jsvi.2001.3923, available online at http://www.idealibrary.com on IDEAL®

DYNAMIC STABILITY OF SKEW PLATES SUBJECTED TO AERODYNAMIC AND RANDOM IN–PLANE FORCES

T. H. Young and C. W. Lee

Department of Mechanical Engineering, National Taiwan University of Science and Technology, Taipei, Taiwan, R.O.C. E-mail: thyoung@mail.ntust.edu.tw

and

F. Y. Chen

Department of Mechanical Engineering, Lee-Ming Institute of Technology, Taisun, Taiwan, R.O.C.

(*Received* 28 *September* 2000, *and in final form* 1 *May* 2001)

This paper presents an investigation into the dynamic stability of skew plates acted upon simultaneously by an aerodynamic force in the chordwise direction and a random in-plane force in the spanwise direction. Due to this random in-plane force, the plate may become unstable before the aerodynamic force reaches its critical value. In this work, the finite element formulation is applied to obtain the discretized system equations. The system equations are then partially uncoupled and reduced in size by the modal truncation method. Finally, the unsmoothed and the smoothed versions of the stochastic averaging are used to calculate the system response, and the second-moment stability criterion is utilized to determine the stability boundary of the system. Numerical results show that the stability boundary obtained by the smoothed stochastic averaging is less conservative than that obtained by the unsmoothed version, and the former is the tangent of the latter at zero spectral density of the random in-plane force.

1. INTRODUCTION

The elastic stability of panels in air flow has been extensively studied by aeroelasticians [1–3]. In most of the references, panels are considered to be acted upon by the aerodynamic force only and to deal primarily with the determination of the critical value of the aerodynamic pressure or of the response amplitude of the limit circle.

In reality, panels may also be subjected to in-plane forces, which are induced by the surrounding structures, in addition to the aerodynamic force. The in-plane forces considered by researchers include static forces, periodic forces and random forces. Dugundji [4] found the exact solution of a simply supported rectangular plate subjected to aerodynamic and static in-plane forces. The critical aerodynamic pressure of a quadrilateral plate acted upon simultaneously by in-plane loads was calculated by Sander *et al.* [5] by using conforming and non-conforming finite elements.

For panels subjected to periodic in-plane forces, Dzygadlo and Kaliski [6] and Dzygadlo [7] determined the stability boundary of a simply supported rectangular plate for subsonic and supersonic air flow. Librescu and Thangjitham [8] examined the dynamic stability of simply supported shear-deformable flat panels subjected to in-plane edge excitation. Recently, the dynamic stability of skew plates acted upon by aerodynamic and periodic in-plane forces was studied by Young and Chen [9, 10]. The aerodynamic force considered

0022-460X/02/080401 + 14 $35.00/0

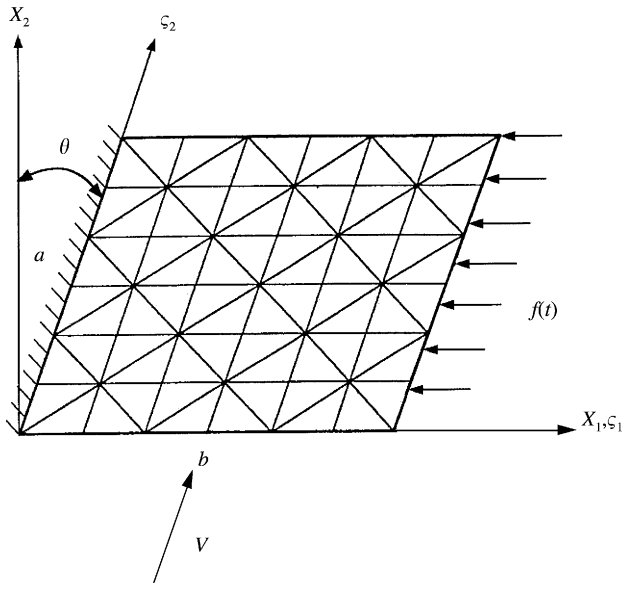

Figure 1. Configuration and finite element mesh of a cantilever skew plate subjected to both aerodynamic and random in-plane forces.

in these two papers is either below or beyond the critical value, and the in-plane force is assumed to act in the spanwise direction different from the direction of the air flow. They found that the in-plane force may, in certain situations, bring about instability before the aerodynamic force reaches its critical value and stabilize the system as the aerodynamic force exceeds its critical value.

The effect of random in-plane loading was investigated by Ibrahim and his students [11, 12] who determined the second-moment stability boundaries and response amplitudes for an infinitely long elastic plate by the moment equation approach. The in-plane loading is assumed as the sum of a constant force and a Gaussian white noise and is acting in the direction of the air flow. Later, Potapov [13] examined the same problem for an infinitely long viscoelastic plate.

This paper studies the dynamic stability of cantilever skew plates subjected simultaneously to an aerodynamic force in the chordwise direction and a random in-plane force in the spanwise direction. The aerodynamic force is modelled by the piston theory, and the random in-plane force is assumed as a physical noise with a zero mean. In this work, the finite element formulation is applied to obtain the discretized system equations. The system equations are then partially uncoupled and reduced in size by the modal truncation method. Finally, the unsmoothed and the smoothed versions of the stochastic averaging are used to calculate the system response, and the second-moment stability criterion is utilized to determine the stability boundary of the system.

2. EQUATION OF MOTION

A cantilever skew plate of side length $a \times b$ with a skew angle θ subjected to both aerodynamic and random in-plane forces is shown in Figure 1. Based on the two-dimensional first order theory (also called the piston theory) [14], the equation of

motion for a thin plate with small-deformation assumption is given by

$$\rho h\ddot{w} - D\nabla^4 w + \left(\beta \frac{\partial w}{\partial \zeta_2} + \mu \dot{w}\right) + f(t)\frac{\partial^2 w}{\partial x_1^2} = 0. \tag{1}$$

In the above equation, w is the transverse displacement; ζ_2 is one of the skew co-ordinates, as shown in Figure 1; ρ, h and D are the mass density, the thickness and the flexural rigidity of the plate, respectively; ∇^4 is a biharmonic operator in Cartesian co-ordinates; the overdot denotes a partial differentiation with respect to time t; the aerodynamic pressure parameter β and damping parameter μ are

$$\beta = 2q/\sqrt{M_\infty^2 - 1} \quad \text{and} \quad \mu = (\beta/V)[(M_\infty^2 - 2)/(M_\infty^2 - 1)],$$

where q is the dynamic pressure, M_∞ is the Mach number, and V is the flow velocity.

The equation of motion, equation (1), is a partial differential equation with time-dependent coefficients, and the problem possesses no exact solutions. Therefore, an approximate method must be utilized to find an analytic solution. In this paper, the finite element method is used to separate the dependence on the spatial co-ordinates first. By use of the three-node, nine-degree-of-freedom triangular element [15], the displacement within an element can be written as

$$w = \mathbf{N}^{\mathrm{T}}\mathbf{d}_e, \tag{2}$$

where the shape function vector $\mathbf{N}$ and the nodal parameter vector $\mathbf{d}_e$ are given in the book by Zienkiewicz [15]. Substituting equation (2) into equation (1), going through the finite element formulations yields the following equation for the discretized system [9]:

$$\frac{\rho h a^4}{D}[M]\ddot{\mathbf{d}} + \frac{\mu a^4}{D}[C]\dot{\mathbf{d}} + [K_b]\mathbf{d} + \frac{\beta a^3}{D}[F_p]\mathbf{d} + \frac{f(t)a^2}{D}[F_i]\mathbf{d} = 0, \tag{3}$$

where $[M]$, $[C]$, and $[K_b]$ are the mass, damping, and stiffness matrices, respectively; $[F_i]$ and $[F_p]$ are the force matrices due to the in-plane and the aerodynamic forces, respectively, and $\mathbf{d}$ is the column matrix formed by all the $\mathbf{d}_e$. Note that the damping matrix $[C]$ is equal to the mass matrix $[M]$ because both ρh and μ are constants.

Equation (3) is a set of simultaneous differential equations with variable coefficients and cannot be solved exactly. To improve the solvability of the system equations, a modal analysis procedure is then applied to decouple the autonomous terms in the equations. In the meantime, since flutter usually occurs among the lowest few modes, a modal truncation is taken during the modal analysis procedure to reduce the size of the system equations. Therefore, introduce a linear transformation

$$\mathbf{d} = [Y]\mathbf{v} \tag{4}$$

where $[Y]$ is a truncated right modal matrix formed by the first J normalized modes of the corresponding undamped, autonomous system, i.e.,

$$\omega_j^2[M]\mathbf{y}_j = ([K_b] + \frac{\beta a^3}{D}[F_p])\mathbf{y}_j \quad \text{and} \quad \mathbf{z}_j^{\mathrm{T}}[M]\mathbf{y}_j = 1, \quad j = 1, 2, \ldots, J \tag{5}$$

in which $\omega_j = \tilde{\omega}_j\sqrt{\rho h a^4/D}$ with $\tilde{\omega}_j$ being the natural frequency of the corresponding undamped, autonomous system; $\mathbf{y}_j$ and $\mathbf{z}_j$ are the right and left eigenvectors of the

corresponding undamped, autonomous system, respectively, since the matrix $[F_p]$ is asymmetric. Note that the random in-plane excitation $f(t)$ is assumed to have a zero mean here; otherwise, the constant part of the in-plane force has to be included in equation (5). Substituting this transformation into equation (3) and premultiplying the transpose of the corresponding truncated left modal matrix $[Z]^{\mathrm{T}}$ formed by the first J normalized modes to the equation yields the following reduced and partially uncoupled form if the aerodynamic pressure parameter β is smaller than its critical value β_{cr}:

$$\frac{\rho h a^4}{D}\ddot{\mathbf{v}} + \frac{\mu a^4}{D}\dot{\mathbf{v}} + [\omega^2]\mathbf{v} + \frac{f(t)a^2}{D}[G]\mathbf{v} = \mathbf{0}, \tag{6}$$

where the matrix $[G] = [Z]^{\mathrm{T}}[F_i][Y]$, and $[\omega^2]$ is a diagonal matrix with each diagonal entry being square of the non-dimensionalized natural frequency. Moreover, the temporal variable is changed such that the differential equation is in terms of the dimensionless variable $\tau = \sqrt{(D/\rho h a^4)}t$. This change transforms equation (6) into the form

$$v_j''(\tau) + 2\alpha v_j'(\tau) + \omega_j^2 v_j(\tau) = -\tilde{f}(\tau)\sum_{r=1}^{J} g_{jr}v_r(\tau), \quad j = 1, \ldots, J, \tag{7}$$

where v_j and g_{jr} are entries of the matrices $\mathbf{v}$ and $[G]$, respectively, "$'$" denotes a differentiation with respect to τ, $\alpha = \mu a^2/2\sqrt{\rho h D}$, and $\tilde{f} = fa^2/D$.

3. THE UNSMOOTHED STOCHASTIC AVERAGING

When the aerodynamic pressure parameter β increases and approaches its critical value β_{cr}, two natural frequencies of the system, say ω_p and ω_q, get close, and the system behavior is dominated by these two modes. Therefore, the system can be approximated by a two-degree-of-freedom system by considering only these two modes, i.e., equation (7) can be rewritten as

$$\begin{aligned} v_p''(\tau) + 2\alpha v_p'(\tau) + \omega_p^2 v_p(\tau) &= -\tilde{f}(\tau)(g_{pp}v_p + g_{pq}v_q), \\ v_q''(\tau) + 2\alpha v_q'(\tau) + \omega_q^2 v_q(\tau) &= -\tilde{f}(\tau)(g_{qp}v_p + g_{qq}v_q). \end{aligned} \tag{8}$$

Letting $[y_1, y_2, y_3, y_4] = [v_p, v_p', v_q, v_q']$, the above equation can be written as a set of first order differential equations,

$$\begin{aligned} y_1' &= G_{10} + G_{11}\tilde{f}(\tau), \qquad y_2' = G_{20} + G_{21}\tilde{f}(\tau), \\ y_3' &= G_{30} + G_{31}\tilde{f}(\tau), \qquad y_4' = G_{40} + G_{41}\tilde{f}(\tau), \end{aligned} \tag{9}$$

where $G_{10} = y_2, \quad G_{11} = 0,$

$$G_{20} = -(2\alpha y_2 + \omega_p^2 y_1), \qquad G_{21} = -(g_{pp}y_1 + g_{pq}y_3),$$

$$G_{30} = y_4, \qquad G_{31} = 0,$$

$$G_{40} = -(2\alpha y_4 + \omega_q^2 y_3), \qquad G_{41} = -(g_{qp}y_1 + g_{qq}y_3).$$

If the relaxation time of the system is much larger than the correlation time of the random in-plane excitation $\tilde{f}(\tau)$, the system response can be approximated as a Markov process governed by the following Ito differential equations [16]:

$$\mathrm{d}y_i = m_i\,\mathrm{d}\tau + \sigma_{ij}\,\mathrm{d}B_j, \quad i,j = 1,\ldots,4, \tag{10}$$

where B_j are mutually independent Wiener processes with a unit variance, m_i and σ_{ij} are the drift and the diffusion coefficients, respectively. If the autocorrelation function of the random in-plane excitation $R_{ff}(\tau)$ is stationary and non-zero only within a small neigborhood around the origin $\tau = 0$, m_i and σ_{ij} can be given by

$$m_i = G_{i0} + \sum_j \int_{-\infty}^{0} \frac{\partial G_{i1}}{\partial y_j}\, G_{j1,\tau^*} R_{ff}(\tau^*)\,\mathrm{d}\tau^*,$$

$$([\sigma][\sigma]^{\mathrm{T}})_{ij} = \int_{-\infty}^{\infty} G_{i1} G_{j1,\tau^*} R_{ff}(\tau^*)\,\mathrm{d}\tau^*, \quad i,j = 1,\ldots,4, \tag{11}$$

where $([\sigma][\sigma]^{\mathrm{T}})_{ij}$ denotes the i–jth entry of the product of the diffusion matrix and its transpose, and $G_{j1,\tau^*}(\cdot) = G_{j1}(\cdot, \tau + \tau^*)$. This is referred to as the unsmoothed version of the stochastic averaging [16]. Assume further that $\tilde{f}(\tau)$ is a delta-correlated noise, i.e.,

$$R_{ff}(\tau^*) = S\delta(\tau^*)$$

where S is the spectral density of $\tilde{f}(\tau)$, and $\delta(\cdot)$ denotes a Dirac delta function. Then the expressions for m_i and the non-zero $([\sigma][\sigma]^{\mathrm{T}})_{ij}$ can be easily calculated as

$$\begin{aligned}
&m_1 = y_2,\\
&m_2 = -\left\{2\alpha y_2 + \omega_p^2 y_1 - \frac{S}{2}\left[(g_{pp}^2 + g_{pq}g_{qp})y_1 + (g_{pp}g_{pq} + g_{pq}g_{qq})y_3\right]\right\},\\
&m_3 = y_4,\\
&m_4 = -\left\{2\alpha y_4 + \omega_q^2 y_3 - \frac{S}{2}\left[(g_{qp}g_{pp} + g_{qq}g_{qp})y_1 + (g_{qp}g_{pq} + g_{qq}^2)y_3\right]\right\},\\
&([\sigma][\sigma]^{\mathrm{T}})_{22} = (g_{pp}y_1 + g_{pq}y_3)^2,\\
&([\sigma][\sigma]^{\mathrm{T}})_{24} = ([\sigma][\sigma]^{\mathrm{T}})_{42} = (g_{pp}y_1 + g_{pq}y_3)(g_{qp}y_1 + g_{qq}y_3),\\
&([\sigma][\sigma]^{\mathrm{T}})_{44} = (g_{qp}y_1 + g_{qq}y_3)^2.
\end{aligned} \tag{12}$$

The above results can also be obtained by the Wong–Zakai convergence theorem [17].

By Ito's differential rule, the stochastic differential equation for $y_i y_j$ may be obtained as

$$\mathrm{d}(y_1 y_j) = (m_i y_j + m_j y_j + \tfrac{1}{2}\sigma_{ik}\sigma_{jk})\mathrm{d}\tau + (\sigma_{ik}y_j + \sigma_{jk}y_i)\,\mathrm{d}B_k, \quad i,j,k = 1,\ldots,4, \tag{13}$$

where a repeated index indicates a summation over its range. Taking the ensemble average yields the following second-order moment equations:

$$\frac{\mathrm{d}}{\mathrm{d}\tau}E[y_1y_2] = -2\alpha E[y_1y_2] + \frac{S}{2}(g_{pq}g_{qq} + g_{pp}g_{pq})E[y_1y_3]$$

$$-\left[\omega_p^2 - \frac{S}{2}(g_{pp}^2 + g_{pq}g_{qp})\right]E[y_1^2] + E[y_2^2],$$

$$\frac{\mathrm{d}}{\mathrm{d}\tau}E[y_1y_3] = E[y_1y_4] + E[y_2y_3],$$

$$\frac{\mathrm{d}}{\mathrm{d}\tau}E[y_1y_4] = -\left[\omega_q^2 - \frac{S}{2}(g_{qq}^2 + g_{qp}g_{pq})\right]E[y_1y_3] - 2\alpha E[y_1y_4] + E[y_2y_4]$$

$$+\frac{S}{2}(g_{qp}g_{pp} + g_{qq}g_{qp})E[y_1^2],$$

$$\frac{\mathrm{d}}{\mathrm{d}\tau}E[y_2y_3] = -\left[\omega_p^2 - \frac{S}{2}(g_{pp}^2 + g_{pq}g_{qp})\right]E[y_1y_3] - 2\alpha E[y_2y_3] + E[y_2y_4]$$

$$+\frac{S}{2}(g_{pq}g_{qq} + g_{pp}g_{pq})E[y_3^2],$$

$$\frac{\mathrm{d}}{\mathrm{d}\tau}E[y_2y_4] = \frac{S}{2}(g_{qp}g_{pp} + g_{qq}g_{qp})E[y_1y_2] + S(g_{pp}g_{qq} + g_{pq}g_{qp})E[y_1y_3]$$

$$-\left[\omega_p^2 - \frac{S}{2}(g_{pp}^2 + g_{pq}g_{qp})\right]E[y_1y_4] - \left[\omega_q^2 - \frac{S}{2}(g_{qq}^2 + g_{qp}g_{pq})\right]$$

$$\times E[y_2y_3] - 4\alpha E[y_2y_4] + \frac{S}{2}(g_{pq}g_{qq} + g_{pp}g_{pq})E[y_3y_4]$$

$$+ Sg_{pp}g_{qp}E[y_1^2] + Sg_{pq}g_{qq}E[y_3^2], \tag{14}$$

$$\frac{\mathrm{d}}{\mathrm{d}\tau}E[y_3y_4] = \frac{S}{2}(g_{qp}g_{pp} + g_{qq}g_{qp})E[y_1y_3] - 2\alpha E[y_3y_4]$$

$$-\left[\omega_q^2 - \frac{S}{2}(g_{qq}^2 + g_{qp}g_{pq})\right]E[y_3^2] + E[y_4^2],$$

$$\frac{\mathrm{d}}{\mathrm{d}\tau}E[y_1^2] = 2E[y_1y_2],$$

$$\frac{\mathrm{d}}{\mathrm{d}\tau}E[y_2^2] = -[2\omega_p^2 - S(g_{pp}^2 + g_{pq}g_{qp})]E[y_1y_2] + 2Sg_{pp}g_{pq}E[y_1y_3]$$

$$+ S(g_{pq}g_{qq} + g_{pp}g_{pq})E[y_2y_3] + Sg_{pp}^2E[y_1^2]$$

$$- 4\alpha E[y_2^2] + Sg_{pq}^2E[y_3^2],$$

$$\frac{\mathrm{d}}{\mathrm{d}\tau}E[y_3^2] = 2E[y_3y_4],$$

$$\frac{\mathrm{d}}{\mathrm{d}\tau}E[y_4^2] = 2Sg_{qp}g_{qq}E[y_1y_3] + S(g_{qp}g_{pp} + g_{qq}g_{qp})E[y_1y_4]$$

$$- [2\omega_q^2 - S(g_{qq}^2 + g_{qp}g_{pq})]E[y_3y_4] + Sg_{qp}^2E[y_1^2]$$

$$+ Sg_{qq}^2E[y_3^2] - 4\alpha E[y_4^2].$$

Letting $e = \{E[y_1y_2], E[y_1y_3], E[y_1y_4], E[y_2y_3], E[y_2y_4], E[y_3y_4], E[y_1^2], E[y_2^2], E[y_3^2], E[y_4^2]\}^{\mathrm{T}}$, the above moment equations can be written as

$$\frac{\mathrm{d}}{\mathrm{d}\tau}e = [H]e, \tag{15}$$

where $[H]$ is a constant square matrix. The sufficient and necessary condition for the system to be stable in the second-moment sense is the real part of all eigenvalues of $[H]$ being negative, from which the second-moment stability boundary of the system can be calculated.

4. THE SMOOTHED STOCHASTIC AVERAGING

The solution of equation (8) can also be assumed to be of the form

$$v_p = u_1\cos\Phi_1 \quad \text{and } v_q = u_2\cos\Phi_2, \tag{16}$$

with $\Phi_1 = \omega_p\tau + \phi_1$ and $\Phi_2 = \omega_q\tau + \phi_2$,

where u_1, u_2, ϕ_1 and ϕ_2 are the amplitudes and phase angles of v_p and v_q, respectively. Under the constraint conditions

$$v_p' = -\omega_p u_1\sin\Phi_1 \quad \text{and} \quad v_q = -\omega_q u_2\sin\Phi_2.$$

u_1, u_2, ϕ_1 and ϕ_2 are found to be

$$u_1' = [F_{10} + F_{11}\tilde{f}(\tau)]\sin\phi_1, \qquad \phi_1' = \frac{1}{u_1}[F_{10} + F_{11}\tilde{f}(\tau)]\cos\phi_1,$$

$$u_2' = [F_{20} + F_{21}\tilde{f}(\tau)]\sin\phi_2, \qquad \phi_2' = \frac{1}{u_2}[F_{20} + F_{21}\tilde{f}(\tau)]\cos\phi_2, \tag{17}$$

where $F_{10} = -2\alpha u_1 \sin\phi_1, \qquad F_{11} = \dfrac{2}{\omega_p}(g_{pp}u_1 \cos\phi_1 + g_{pq}u_2 \cos\phi_2),$

$$F_{20} = -2\alpha u_2 \sin\phi_2, \qquad F_{21} = \frac{2}{\omega_q}(g_{qp}u_1 \cos\phi_1 + g_{qq}u_2 \cos\phi_2).$$

If the right-hand side of equation (17) is small in some sense, the smoothed version of stochastic averaging can be applied to obtain the Ito differential equation governing the solution of the equation. Based on the Khas'minskii limit theorem [18], the solution of equation (17) converges weakly to a Markov process which is governed by the following Ito differential equations:

$$\mathrm{d}u_1 = m_1\,\mathrm{d}\tau + \sigma_{11}\,\mathrm{d}B_1 + \sigma_{12}\,\mathrm{d}B_2, \qquad \mathrm{d}u_2 = m_2\,\mathrm{d}\tau + \sigma_{21}\,\mathrm{d}B_1 + \sigma_{22}\,\mathrm{d}B_2, \tag{18}$$

where B_1 and B_2 denote mutually independent Wiener processes with a unit variance, and the drift coefficients m_i and the diffusion coefficients σ_{ij} are given by

$$m_i = \left\langle F_{i0}\sin\phi_i + \sum_j \int_{-\infty}^{0} \left[\frac{\partial F_{i1}}{\partial u_j} F_{j1,\tau^*}\sin\phi_i \sin\phi_{j,\tau^*} + \frac{1}{u_j}\frac{\partial F_{i1}}{\partial \phi_j} F_{j1,\tau^*}\sin\phi_i\cos\phi_{j,\tau^*}\right] \times R_{ff}(\tau^*)\,\mathrm{d}\tau^* \right\rangle,$$

$$([\sigma][\sigma]^{\mathrm{T}})_{ij} = \left\langle \int_{-\infty}^{\infty} F_{i1}F_{j1,\tau^*}\sin\phi_i\sin\phi_{j,\tau^*}R_{ff}(\tau^*)\,\mathrm{d}\tau^* \right\rangle, \quad i,j = 1,2, \tag{19}$$

where the symbol $\langle[\cdot]\rangle$ represents the time-averaging operation, i.e.,

$$\langle[\cdot]\rangle = \lim_{T\to\infty}\frac{1}{2T}\int_{-T}^{T}[\cdot]\,\mathrm{d}\tau.$$

Expressions for m_i and $([\sigma][\sigma]^{\mathrm{T}})_{ij}$ are found to be

$$m_1 = -\alpha u_1 + \left(\frac{3g_{pp}^2 u_1}{4} + \frac{g_{pq}^2 u_2^2}{2u_1}\right)\frac{S}{\omega_p^2},$$

$$m_2 = -\alpha u_2 + \left(\frac{3g_{qq}^2 u_2}{4} + \frac{g_{qp}^2 u_1^2}{2u_2}\right)\frac{S}{\omega_q^2},$$

$$([\sigma][\sigma]^{\mathrm{T}})_{11} = \left[\frac{S}{4\omega_p^2}(g_{pp}^2u_1^2 + 2g_{pq}^2u_2^2)\right], \tag{20}$$

$$([\sigma][\sigma]^{\mathrm{T}})_{22} = \left[\frac{S}{4\omega_q^2}(g_{qq}^2u_2^2 + 2g_{qp}^2u_1^2)\right],$$

$$([\sigma][\sigma]^{\mathrm{T}})_{12} = ([\sigma][\sigma]^{\mathrm{T}})_{21} = 0.$$

By using equation (18), the Ito differential equations for u_1^2 and u_2^2 can be acquired. Then taking the expectation on both sides of the equations yields

$$\begin{Bmatrix} \dfrac{\mathrm{d}}{\mathrm{d}\tau} E[u_1^2] \\ \dfrac{\mathrm{d}}{\mathrm{d}\tau} E[u_2^2] \end{Bmatrix} = \begin{bmatrix} A_{11} & A_{12} \\ A_{21} & A_{22} \end{bmatrix} \begin{Bmatrix} E[u_1^2] \\ E[u_2^2] \end{Bmatrix}, \tag{21}$$

where the elements of the matrix

$$A_{11} = -2\alpha + \frac{g_{pp}^2}{2\omega_p^2} S, \qquad A_{12} = \frac{g_{pq}^2}{2\omega_p^2} S,$$

$$A_{21} = \frac{g_{qp}^2}{2\omega_q^2} S, \qquad A_{22} = -2\alpha + \frac{g_{qq}^2}{2\omega_q^2} S,$$

The stability of equation (21) can be assured if all the real parts of eigenvalues of the coefficient matrix are negative, which can be satisfied by the following conditions:

$$2\alpha - \frac{g_{pp}^2}{2\omega_p^2} S \geqslant 0, \qquad 2a - \frac{g_{qq}^2}{2\omega_q^2} S \geqslant 0,$$

$$\left(2\alpha - \frac{g_{pp}^2}{2\omega_p^2} S\right)\left(2\alpha - \frac{g_{qq}^2}{2\omega_q^2} S\right) \geqslant \left(\frac{g_{pq} g_{qp}}{2\omega_p \omega_q} S\right)^2. \tag{22}$$

These three conditions can all be satisfied if

$$\alpha \geqslant \frac{S}{8}\left\{\left(\frac{g_{pp}^2}{\omega_p^2} + \frac{g_{qq}^2}{\omega_q^2}\right) + \left[\left(\frac{g_{pp}^2}{\omega_p^2} - \frac{g_{qq}^2}{\omega_q^2}\right)^2 + \frac{4 g_{pq}^2 g_{qp}^2}{\omega_p^2 \omega_q^2}\right]^{1/2}\right\}. \tag{23}$$

It is observed from the above equation that the critical value of α is proportional to S by the second-moment stability criterion, which means that the second-moment stability boundary of the system is a straight line on the S–α plane.

5. NUMERICAL RESULTS AND DISCUSSIONS

Before formally presenting the numerical results for stability studies, flutter analysis of the system defined by equation (5) must be conducted first. According to the previous study [9], the finite element mesh is shown in Figure 1 with 126 degrees of freedom, and the number of modes used in the mode truncation method is taken as 30 in this work. Moreover, for a cantilever skew plate with aspect ratio $a/b = 1$, it is found that flutter occurs between the first and second modes for skew angles up to 30°.

Before the aerodynamic pressure parameter reaches its critical value, the plate is still stable if subjected to the aerodynamic force alone. In this situation, if the plate is subjected to a random in-plane excitation in addition to the aerodynamic force, it may become unstable according to the previous analysis. Figure 2 presents the second-moment stability boundaries of a cantilever square plate acted upon by an aerodynamic force in the chordwise direction and a random in-plane force in the spanwise direction in the S–α plane.

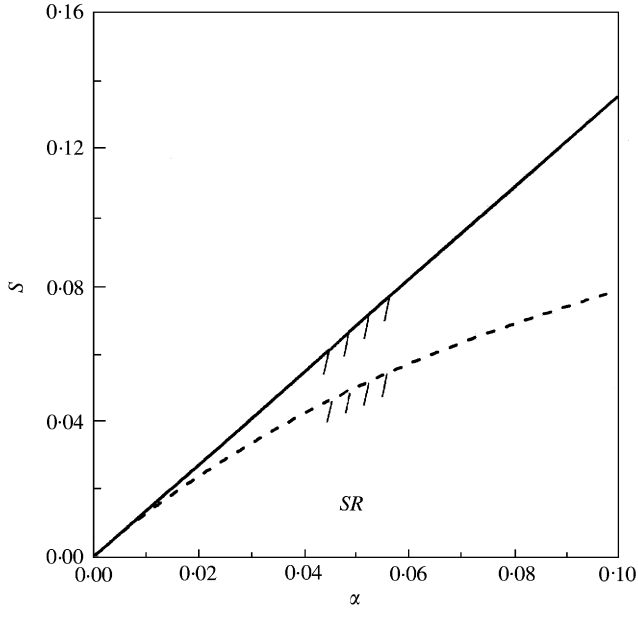

Figure 2. Stability boundaries of a cantilever square plate acted upon by both aerodynamic and random in-plane forces in the S–α plane. $\nu = 0{\cdot}3$, $\beta/\beta_{cr} = 0{\cdot}95$: ————, smoothed version; – – – – –, unsmoothed version.

The boundary obtained by the smoothed stochastic averaging is a straight line, as predicted in the above section, while the boundary obtained by the unsmoothed stochastic averaging is a curve. It is observed that the straight line is the tangent of the curve at the origin. Therefore, for a small spectral density of the random excitation, the solution obtained from the smoothed stochastic averaging is the best approximation to that of the unsmoothed stochastic averaging. The stable region (SR) lies beneath the stability boundary, and hence the stability boundary calculated from the unsmoothed stochastic averaging is more conservative than that from the smoothed stochastic averaging.

Figure 3 shows the effect of aerodynamic pressure on the second-moment stability boundary of the cantilever square plate as considered in Figure 2. Figure 3(a) shows the stability boundaries obtained by the unsmoothed stochastic averaging, and Figure 3(b) shows the stability boundaries obtained by the smoothed stochastic averaging. All the stability boundaries start from the origin because in the absence of the random in-plane excitation, the plate is still stable if the aerodynamic pressure does not exceed the critical value. The figure also reveals that an increase in the aerodynamic pressure will lower the stability boundary, leaving a smaller stability region. This is attributed to the fact that a larger aerodynamic pressure pushes the system closer to the unstable configuration. Consequently, it needs a smaller random in-plane excitation to force the system to be unstable.

The effect of damping on the second-moment stability boundary of the cantilever square plate as considered in the previous figure is depicted in Figure 4. All the stability boundaries in Figures 4(a) and 4(b) end at the lower right corner of the figure, at which $\beta/\beta_{cr} = 1{\cdot}0$, because in the absence of the random in-plane excitation, the plate becomes unstable as the aerodynamic pressure reaches its critical value. The figure also shows that a larger damping factor α corresponds to a higher stability boundary and results in a larger stability region. Actually, a larger damping consumes more energy from the system, which needs a stronger

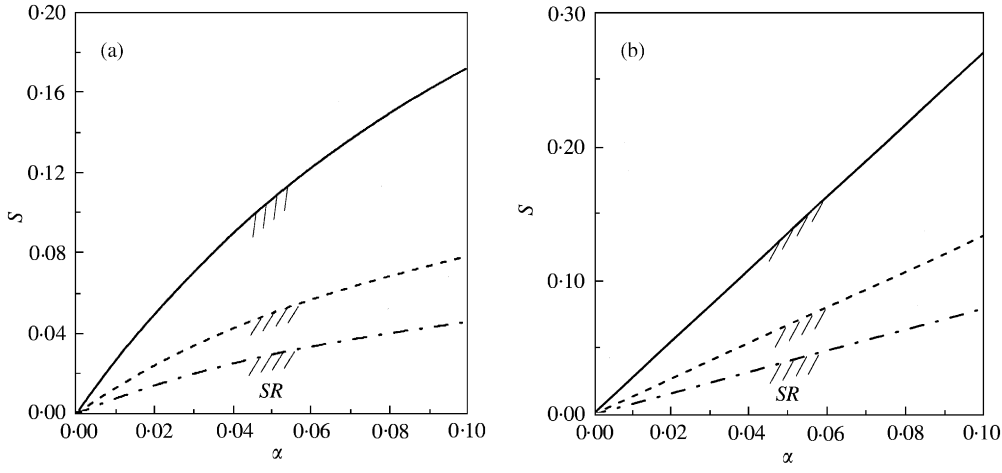

Figure 3. The effect of aerodynamic pressure on the second-moment stability boundaries of a cantilever square plate, $\nu = 0{\cdot}3$: (a) the unsmoothed averaging; (b) the smoothed averaging: ————, $\beta/\beta_{cr} = 0{\cdot}90$; – – – – –, $\beta/\beta_{cr} = 0{\cdot}95$; · – · – · –, $\beta/\beta_{cr} = 0{\cdot}97$.

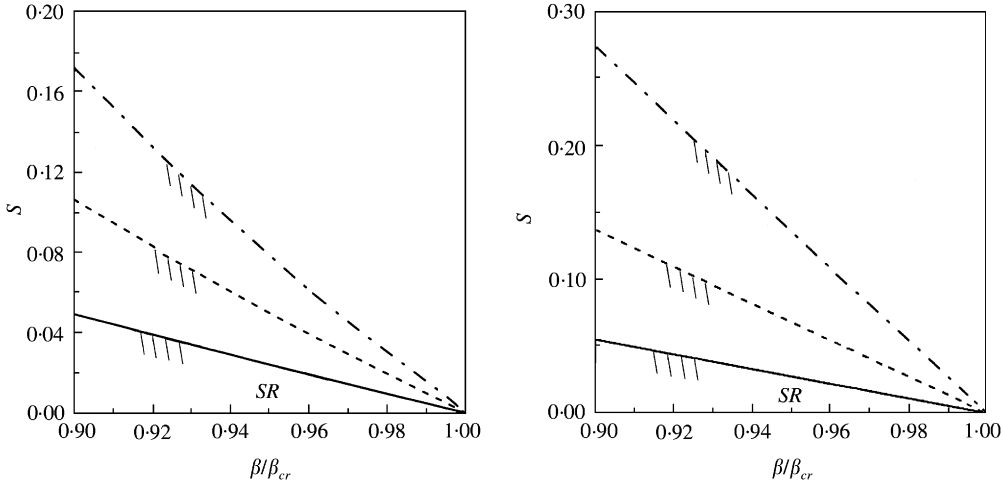

Figure 4. The effect of damping on the second-moment stability boundaries of a cantilever square plate, $\nu = 0{\cdot}3$: (a) the unsmoothed averaging; (b) the smoothed averaging: ————, $\alpha = 0{\cdot}02$; – – – – –, $\alpha = 0{\cdot}05$; · – · – · –, $\alpha = 0{\cdot}1$.

random in-plane excitation to destabilize the system. Therefore, the effect of damping is favourable in this case.

The effect of the spectral density of the random in-plane excitation on the second-moment stability boundary of the same square plate is illustrated in Figure 5. Note that the stability boundaries, obtained by the smoothed stochastic averaging, in Figure 5(b) are not straight lines any more. All the stability boundaries in both figures rise quickly and approach the horizontal line $\beta/\beta_{cr} = 1{\cdot}0$ as the damping factor α increases. This shows that as the aerodynamic pressure is well below its critical value, stability of the plate is mainly decided by the damping and random in-plane excitation. However, if the aerodynamic pressure is very close to its critical value, stability of the plate is predominantly affected by

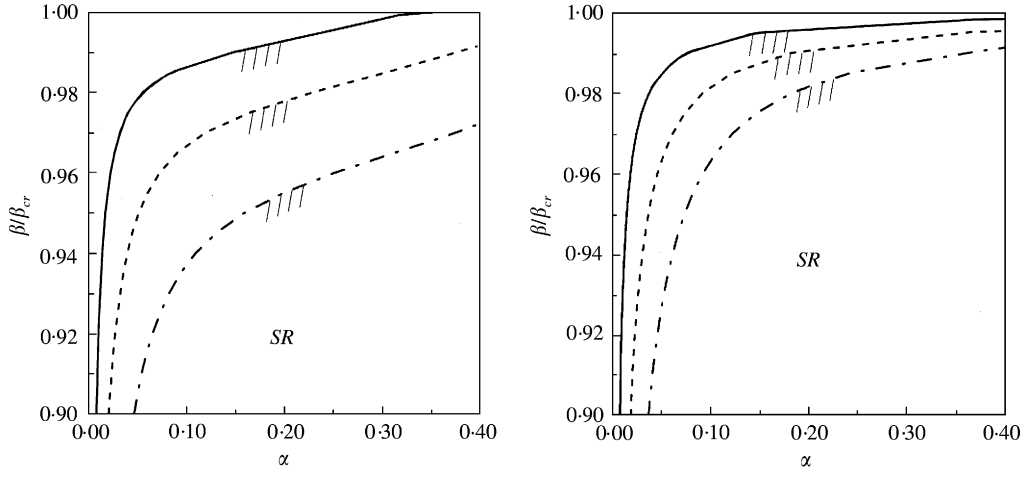

Figure 5. The effect of the spectral density of the random in-plane excitation on the second-moment stability boundaries of a cantilever square plate, $\nu = 0{\cdot}3$: (a) the unsmoothed averaging; (b) the smoothed averaging: ————, $S = 0{\cdot}02$; – – – – –, $S = 0{\cdot}05$; · – · – · – ·, $S = 0{\cdot}1$.

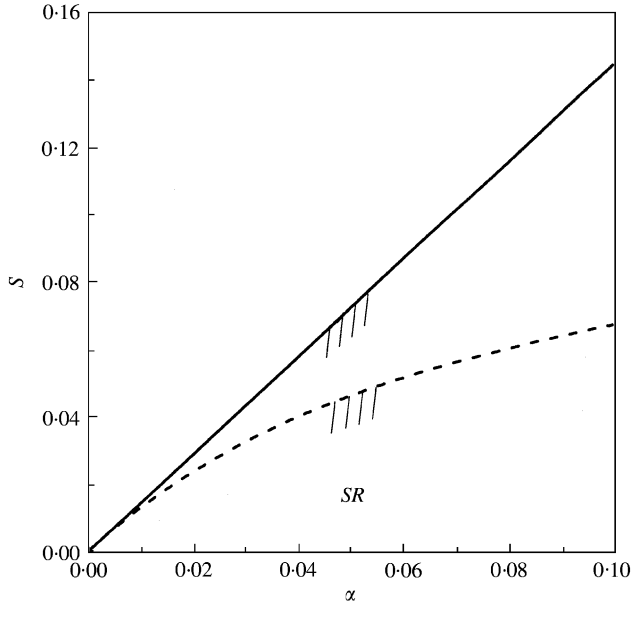

Figure 6. Stability boundaries of a cantilever skew plate acted upon by both aerodynamic and random in-plane forces in the S–α plane, $a/b = 1{\cdot}0$, $\nu = 0{\cdot}3$, $\theta = 30^\circ$ and $\beta/\beta_{cr} = 0{\cdot}95$: ————, smoothed version; – – – – –, unsmoothed version.

the random in-plane excitation and the aerodynamic pressure itself. Above the line, the system is unstable even if the random in-plane excitation is absent. It is found from the figure that a larger spectral density corresponds to a lower stability boundary, leaving a smaller stability region. Therefore, the effect of the spectral density of the random in-plane excitation is destabilizing in this situation.

Figure 6 presents the second-moment stability boundaries of a cantilever skew plate subjected to both aerodynamic and random in-plane forces in the S–α plane. Although this

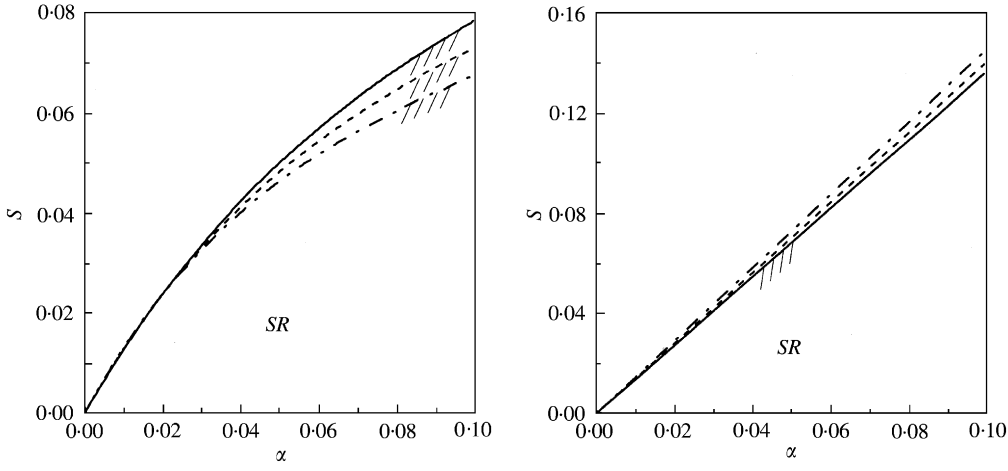

Figure 7. The effect of the skew angle on the second-moment stability boundaries of a cantilever skew plate, $a/b = 1{\cdot}0$, $\nu = 0{\cdot}3$ and $\beta/\beta_{cr} = 0{\cdot}95$: (a) the unsmoothed averaging; (b) the smoothed averaging: ————, $\theta = 0°$; – – – – –, $\theta = 15°$; · – · – · – ·, $\theta = 30°$.

is a skew plate, not a square plate as studied in Figure 2, the stability boundary obtained by the smoothed stochastic averaging is a straight line and is again tangential to that obtained by the unsmoothed stochastic averaging at the origin. Also, the stability boundary calculated from the unsmoothed stochastic averaging is more conservative than that from the smoothed stochastic averaging.

Figure 7 shows the effect of the skew angle on the second-moment stability boundary of the cantilever skew plate considered in Figure 6. Again the stability boundaries in Figure 7(a) are obtained by the unsmoothed stochastic averaging, and those in Figure 7(b) are obtained by the smoothed stochastic averaging. All the stability boundaries in both Figures 7(a) and 7(b) start from the origin because of the same reason as previously mentioned in Figure 3. In Figure 7(b) a larger skew angle corresponds to a steeper stability boundary, leaving a larger stability region. Therefore, the effect of the skew angle is stabilizing if predicted by the smoothed stochastic averaging. However, it is not always true in Figure 7(a) in which the stability boundary is a little bit higher for a larger skew angle at smaller values of α but is visibly lower for a larger skew angle at larger values of α. Therefore, the effect of the skew angle is favorable but not very significant at smaller values of α, and is unfavorable at larger values of α. The reason for this is: in Figure 7(a), as the skew angle increases from 0 to 30°, the stability boundaries bend more, that is, the curvatures of the boundaries at the origin get larger. Hence, the tangents of the boundaries at the origin become steeper for a smaller skew angle, and this is the result shown in Figure 7(b).

6. CONCLUSIONS

The dynamic stability of a cantilever skew plate subjected simultaneously to a sub-critical aerodynamic pressure in the chordwise direction and a random in-plane excitation in the spanwise direction was studied in this paper. The unsmoothed and the smoothed versions of the stochastic averaging are used to calculate the system response. Parametric instability in the second-moment sense was shown to arise due to the random in-plane force before the aerodynamic pressure parameter reaches its critical value.

Numerical results show that the stability boundary obtained by the smoothed stochastic averaging is less conservative than that by the unsmoothed version, and the former is the tangent of the latter at zero spectral density of the random in-plane force. The effects of system parameters on changes of the second-moment stability boundaries of the system were studied. It is found that the effect of damping is stabilizing, while the effects of the aerodynamic pressure and the spectral density of the random in-plane excitation are unfavorable to the second-moment stability of the system. For skew plates, the effect of the skew angle is quite complicated. It depends not only on the aerodynamic pressure and the damping factor of the plate but also on the method applied to obtain the system response.

REFERENCES

1. Y. C. FUNG 1963 *American Institute of Aeronautics and Astronautics Journal* **1**, 898–909. Some recent contributions to panel flutter research.
2. E. H. DOWELL 1970 *American Institute of Aeronautics and Astronautics Journal* **8**, 385–399. A review of the aeroelastic stability of plate and shell.
3. E. H. DOWELL 1975 *Aeroelasticity of Plate and Shell*. Leyden: Noordhoff Int. Pub.
4. J. DUGUNDJI 1966 *American Institute of Aeronautics and Astronautics Journal* **4**, 1257–1266. Theoretical considerations of panel flutter at high supersonic mach numbers.
5. G. SANDER, C. BON and M. GERADIN 1973 *Journal for Numerical Methods in Engineering* **7**, 379–394. Finite element analysis of supersonic panel flutter.
6. Z. DZYGADLO and S. KALISKI 1966 *Bulletin de L'Academie Polonaise des Sciences Serie des Sciences Techniques* **XIV**, 1–10. Parametric and self-excited vibrations of elastic and aeroelastic systems with traveling waves.
7. Z. DZYGADLO 1965 *Proceedings of Vibration Problems* **4**, 353–365. Parametric self-excited vibrations of a simply supported plate in supersonic flow.
8. L. LIBRESCU and S. THANGJITHAM 1989 *Proceedings of the Thirtieth Structures, Structural Dynamics and Material Conference*: *Part* 1, *Paper No*. 89-12-6-CP. Nonlinear dynamic stability of parametrically-excited shear deformable flat panels.
9. T. H. YOUNG and F. Y. CHEN 1994 *Journal of Sound and Vibration* **171**, 603–615. Stability of skew plates subjected to aerodynamic and in-plane forces.
10. T. H. YOUNG and F. Y. CHEN 1993 *American Institute of Aeronautics and Astronautics Journal* **31**, 1667–1673. Stability of fluttered panels subjected to in-plane harmonic forces.
11. R. A. IBRAHIM, P. O. ORONO and S. R. MADABOOSI 1990 *American Institute of Aeronautics and Astronautics Journal* **28**, 694–702. Stochastic flutter of a panel subjected to random in-plane forces, Part I: two mode interaction.
12. R. A. IBRAHIM and P. O. ORONO 1991 *International Journal of Non-Linear Mechanics* **26**, 867–883. Stochastic non-linear flutter of a panel subjected to random in-plane forces.
13. V. D. POTAPOV 1995 *American Institute of Aeronautics and Astronautics Journal* **33**, 712–715. Stability of viscoelastic plate in supersonic flow under random loading.
14. R. L. BISPLINGHOFF and H. ASHLEY 1962 *Principles of Aeroelasticity*. New York: John Wiley and Sons, Inc.
15. O. C. ZIENKIEWICZ 1977 *The Finite Element Method*. Berkshire: McGraw-Hill Book Co. (UK) Ltd.
16. Y. K. LIN and G. Q. CAI 1995 *Probabilistic Structural Dynamics*. New York: McGraw-Hill, Inc.
17. E. WANG and M. ZAKAI 1965 *International Journal of Engineering Science* **3**, 213–229. On the relation between ordinary and stochastic differential equation.
18. R. Z. KHAS'MINSKII 1966 *Theory of Probability and Its Applications* **11**, 390–406. A limit theorem for the solutions of differential equations with random right-hand sides.